Using Cylindrical Domains of Block Copolymers To Self-Assemble and Align Metallic Nanowires

Jinan Chai[†,‡] and Jillian M. Buriak[†,§,*]

[†]National Institute for Nanotechnology (NINT), National Research Council, 11421 Saskatchewan Drive, Edmonton, Alberta, Canada T6G 2M9, [‡]Department of Mechanical Engineering, University of Alberta, Edmonton, Alberta, Canada T6G 2G8, and [§]Department of Chemistry, University of Alberta, Edmonton, Alberta, Canada T6G 2G2

ABSTRACT Block copolymer thin films can be used as soft templates for a wide range of surfaces where large area patterns of nanoscale features are desired. The cylindrical domains of acid-sensitive, self-assembled monolayers of polystyrene—poly(2-vinylpyridine) block copolymers on silicon surfaces were utilized as structural elements for the production of parallel metal nanowires. Metal ion loading of the P2VP block with simple aqueous solutions of anionic metal complexes is accomplished *via* protonation of this basic block, rendering it cationic; electrostatic attraction leads to a high local concentration of metal complexes within the protonated P2VP domain. A subsequent brief plasma treatment simultaneously removes the polymer and produces metallic nanowires. The morphology of the patterns can modulated by controlling solution concentration, deposition time, and molecular weight of the block copolymers, as well as other factors. Horizontal metallic nanoarrays can be aligned on e-beam lithographically defined silicon substrates within different shapes, *via* graphoepitaxy. This method is highly versatile as the procedures to manipulate nanowire composition, dimension, spacing, and orientation are straightforward and based upon efficient aqueous inorganic chemistry.

KEYWORDS: self-assembly · nanowire · block copolymers · metallization · graphoepitaxy

Metal nanostructures continue to be the focus of intense research because of their fascinating properties that can be distinctly different from those of their bulk counterparts, and thus they show great promise for a range of applications.[1–12] High aspect ratio, one-dimensional (1D) metal nanowires are emerging as important building blocks for on-chip interconnects and active components in nanoscale electronic, magnetic, photonic, and biosensing devices, for instance.[13–24] One of the key ingredients required for these future applications is the ability to integrate numerous 1D addressable nanostructures through assembly, patterning, and alignment on technologically relevant solid supports, such as semiconductor surfaces.[25–32] The challenge lies in fabricating large areas of high-density metallic nanostructures, with feature sizes below 100 nm, in an economically feasible manner. While photolithography will justifiably remain a core technology with respect to upcoming, sub-65 nm nodes on the semiconductor industry association roadmap, cost considerations for mass manufacturing may be one potential constraint.[33–38] As a result, there is interest in the development of complementary patterning strategies that involve large-scale self-assembly, for use as a soft organic template for metal nanostructure development.

Template-assisted fabrication of metallic nanostructures, constructing increasingly small features in parallel, with nanoscale accuracy and minimal expense, has been carried out in a variety of ways. For instance, polycarbonate, alumina, and mesoporous silica membranes containing cylindrical pores, as well as liquid crystal and carbon nanotube arrays, have seen much use as templates to form hexagonal close-packed arrays of vertical nanowires.[39–46] In another approach, Penner's group pioneered electrodeposition along step-edges on oriented pyrolytic graphite to obtain horizontal metal nanowires on this surface.[47–50] Over the past decade, however, self-assembled block copolymer nanostructures for utilization as templates for formation of features with dimensions in the range of 10–100 nm have become increasingly viable due to the compatability of these materials with silicon fabrication, their commercialization, and the numerous reviews and literature reports published by the macromolecular community that have attracted the attention of researchers in other areas.[51–70] Block copolymers are comprised of covalently bound, chemically distinct polymers, and an enormous range have been described and characterized. The resulting self-assembled pattern formed is determined by the volume fraction of the components, and the sizes of the nanoscopic domains are defined by the

Ⓦ This paper contains enhanced objects available on the Internet at http://pubs.acs.org/journals/ancac3.

*Address correspondence to jburiak@ualberta.ca.

Received for review November 2, 2007 and accepted January 16, 2008.

Published online February 5, 2008.
10.1021/nn700341s CCC: $40.75

molecular weight of the copolymer and the strength of the segmental interaction between the blocks.[71–82] As a result, the size and morphology of the block copolymer template can be tuned within a broad spectrum.

A number of methods have been described to produce reduced metal nanoparticles in the self-assembled block copolymer domains by *ex situ* or *in situ* methods. Through an *ex situ* approach, metallic nanoparticles have been capped with monolayers that favor solubilization in one block over the other, to produce nanopatterned block copolymer-supported arrays.[83–88] For instance, Kramer and co-workers employed a symmetric poly(styrene-*block*-2-vinylpyridine) (PS-*b*-P2VP) template to localize gold nanoparticles within PS or PVP domains by coating Au nanoparticles with either thiol-terminated PS or PVP ligands.[83] *In situ* preparation of metallic nanoclusters, using the block copolymers as a nanopatterned reactive medium, has also been outlined.[89–96] Metal ions embedded within one phase of the segregated block copolymer template have been reduced to metal nanoparticles *via* plasma, chemical reducing agents, hydrogen gas exposure, and thermal decomposition.[97–110] The majority of the metallic nanostructures prepared by this method have been spherical nanoparticles or nanorods supported within vertical block copolymer cylinders on surfaces.

In this paper, we outline in detail the *in situ* synthesis of patterned and aligned linear metallic patterns, prepared from block copolymer domains oriented in a parallel fashion to the surface on silicon. This mainly wet chemical block copolymer approach toward the assembly of aligned linear patterns of gold, palladium, and platinum, using PS-*b*-P2VP as a template, was recently introduced,[111] and here we explore the range of synthetic variables, including deposition parameters to control the spacing, width, and height of the resulting nanowires, the nanowire composition, which has been extended to copper and magnetic materials (nickel, cobalt, and iron), and the influence of shape during graphoepitaxy. A diverse array of nanostructures can be easily prepared *via* this approach.

RESULTS AND DISCUSSION

Synthesis of Platinum and Other Metal Nanostructures. A fingerprint structure of cylindrical block copolymers oriented in a parallel fashion to the surface was self-assembled on a clean native oxide-capped Si(100) wafer[112] *via* spin-coating of a PS-*b*-P2VP block copolymer, followed by thermal annealing at 230 °C, well above the glass transition temperature of both polymer blocks, as outlined in Scheme 1. The first PS-P2VP polymer chosen, with a molecular weight of PS(32500)-*b*-P2VP(12000), resulted in cylindrical domains with a center-to-center spacing of approximately 36 nm and a few hundreds of nanometers to micrometers in length. When the fingerprint structure of a monolayer of PS-*b*-P2VP cylinders was immersed into a 10 mM $Na_2[PtCl_4]$(aq) solution in the presence of 0.9% HCl(aq) for 24 h, followed by a 30 s oxygen plasma exposure,[58,113] platinum lines were observed on the silicon surface, as shown in the scanning electron microscopy (SEM) images in Figure 1a,b; the polymer is removed concomitantly *via* the plasma exposure. The width of the lines is ~12 nm, and the height, as determined by atomic force microscopy (AFM; Figure 1c,d), is ~16 nm. Both SEM and AFM reveal that the center-to-center spacing of the Pt lines is about 36 nm, identical to that of the parent block copolymer template. Scanning Auger microscopy (SAM) was utilized to obtain compositional maps of these interfaces, as shown in Figure 1e, and supports the conclusions that the observed features are indeed platinum. The spacing of the metallic features can be controlled *via* utilization of block copolymers of different molecular weights. Figure 2

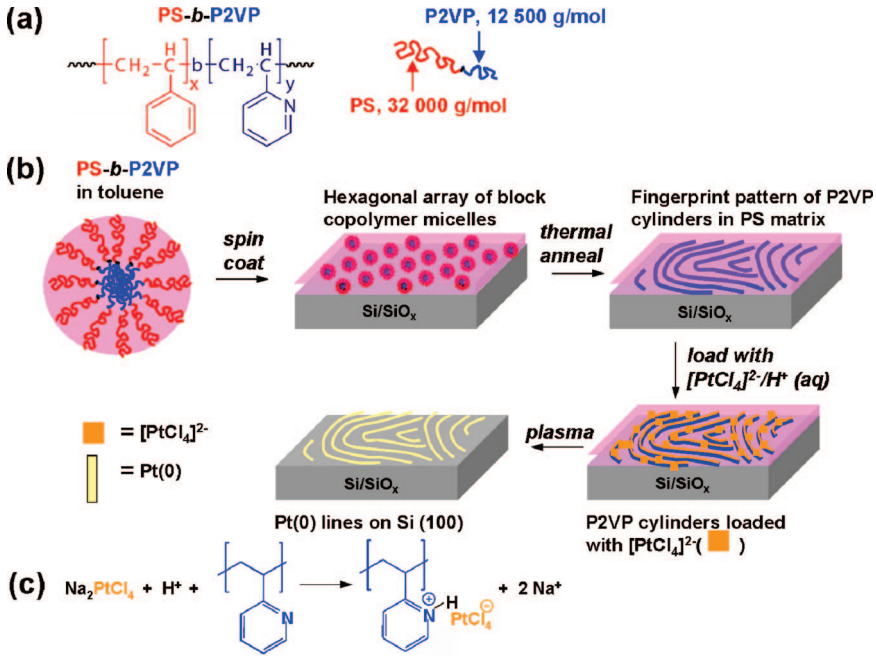

Scheme 1. (a) Structure and molecular weight of the PS-*b*-P2VP block copolymer. (b) A toluene solution containing polymer micelles is spin-coated onto a native oxide-coated silicon surface, forming pseudohexagonal arrays. Thermal annealing of the thin-film-coated wafer shard leads to a fingerprint pattern with P2VP cylinders embedded within the PS matrix. Immersion of the shard in an acidic solution leads to P2VP swelling as a result of protonation; the cationic, protonated P2VP layer then pierces the PS layer. When anionic metallic salts are added to the solution, the positively charged P2VP layer becomes loaded with the metal salts, bound through electrostatic attraction. The polymer is then removed upon plasma treatment, resulting in the formation of "bare" metal wires on the surface. (c) Coordination of anionic metal ions with the P2VP block, in an acidic environment.

shows the SEM images of patterned platinum nanowires with spacings of ~24 and ~42 nm, using PS(23600)-*b*-P2VP(10400) and PS(50000)-*b*-P2VP(16500), respectively.

Modulation of the resulting metal structures can be attained through simple modification of the synthetic parameters involved in metal absorption by the block copolymer monolayer on the silicon surface: modulation of immersion time and metallic ion concentration allows access to different wire continuity and dimensions. Figure 3 shows the SEM images of platinum patterns on Si(100), obtained for a range of concentrations of $Na_2[PtCl_4]$(aq) with 1% HCl(aq) for 1 and 3 h. As can be seen in Figure 3a, the brightness contrast of the linear structures varies, revealing non-uniform platinum deposition at a lower concentration of 0.1 mM for $Na_2[PtCl_4]$, for 1 h of deposition. The inset clearly shows discontinuity along the length of the platinum line. The resulting Pt nanostructures are increasingly uniform in appearance along the length of the lines when the concentration of $Na_2[PtCl_4]$ is increased to 1 and 10 mM (1 h deposition), as shown in Figure 3b,c. Immersion time also plays a critical role, as can be seen by comparing 1 h immersion results (Figure 3a−c) with those for 3 h (Figure 3d−f). The lack of deposition in areas of the patterns in Figure 3a−c is due to incomplete pattern transfer for 1 h of soaking, whereas Figure 3d−f shows complete pattern transfer from the polymer template, resulting in defect-free arrays of platinum lines, after a longer immersion time of 3 h. Although some discontinuity is still observed at the lower $[PtCl_4]^{2-}$ concentration of 0.1 mM (Figure 3d), Figure 3e,f shows uniform pattern transfer over the entire surface at $Na_2[PtCl_4]$ concentrations of 1 and 10 mM. AFM analysis of the same samples shown in Figure 3 (1 h immersion, Figure 4a−c; and 3 h immersion, Figure 4d−f) provides complementary

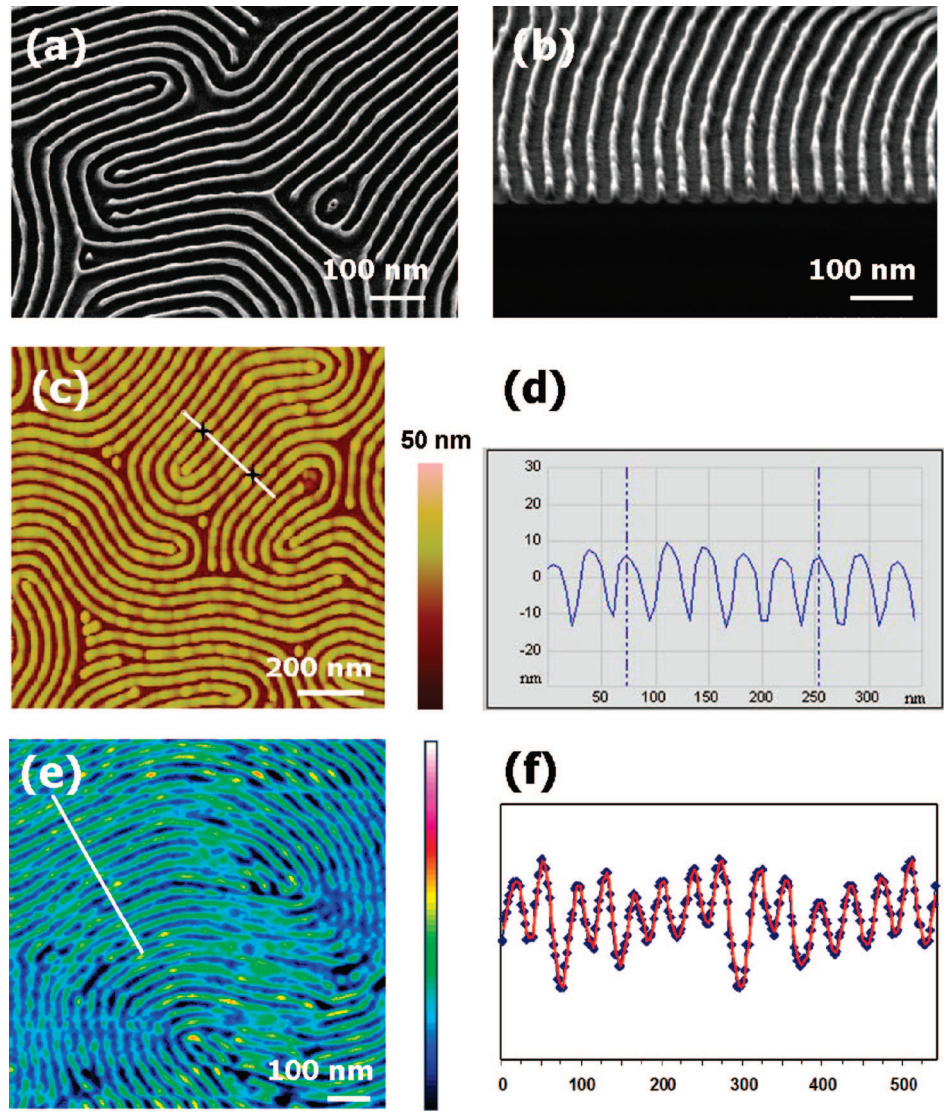

Figure 1. SEM, AFM, and SAM images of platinum nanowires self-assembled after deposition of annealed PS-*b*-P2VP in a 10 mM Na_2PtCl_4/0.9% HCl(aq) solution for 24 h, followed by 30 s oxygen plasma treatment. (a) Plan view SEM image. (b) Cross-sectional SEM image. (c) AFM height image. (d) Cross-sectional AFM analysis. (e) SAM mapping. (f) SAM line profile of platinum NVV.

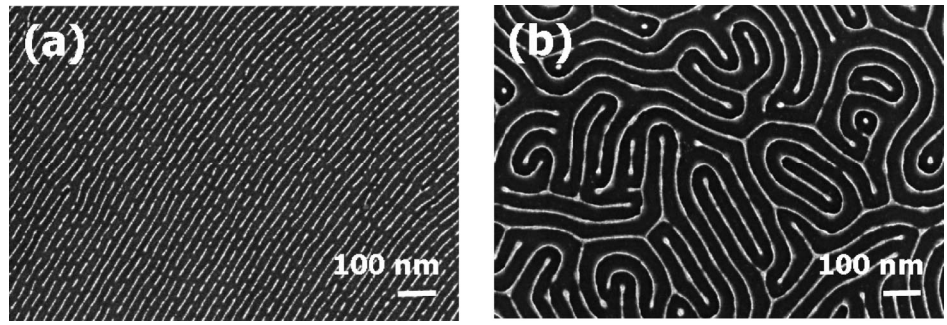

Figure 2. SEM images of platinum nanostructures formed by using templates of different block copolymers of (a) PS(23600)-*b*-P4VP(10400) and (b) PS(50000)-*b*-P4VP(16500) after immersion of the annealed polymer films in 10 mM Na_2PtCl_4/0.9% HCl(aq) for 3 h, followed by plasma treatment.

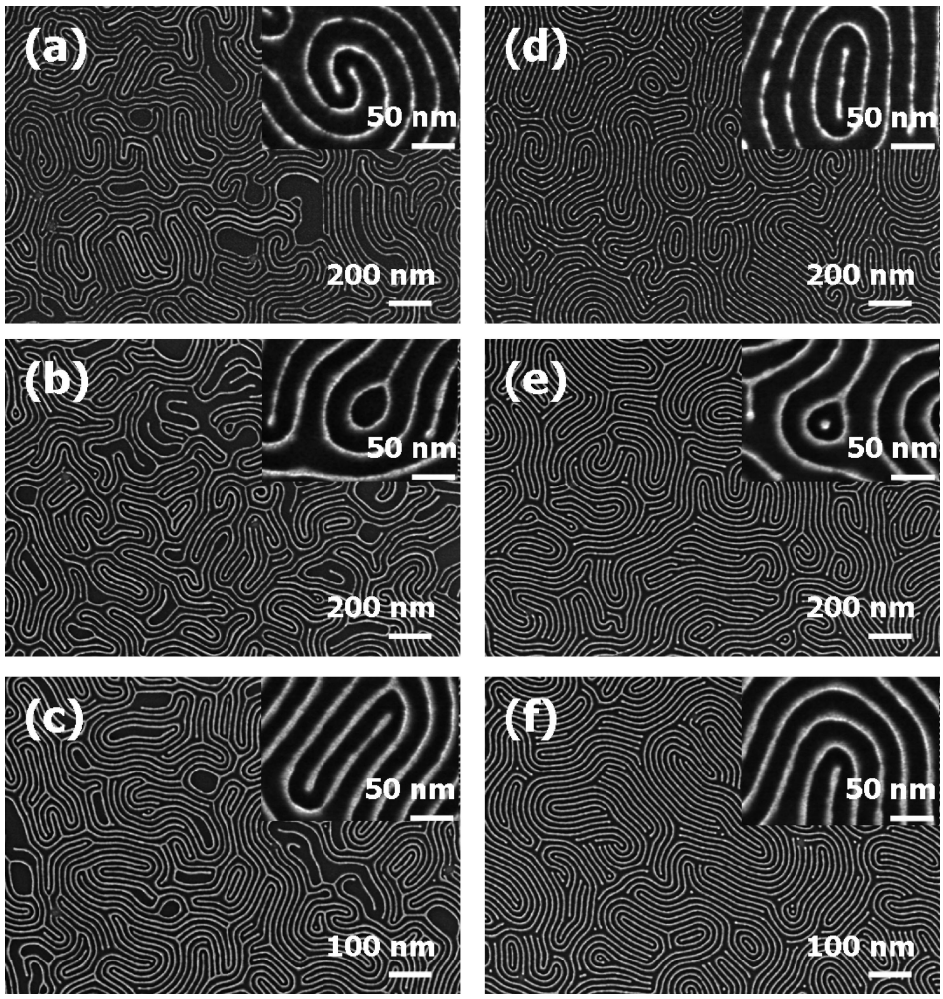

Figure 3. SEM images of platinum wires prepared under the following conditions: (a) 0.1 mM Na_2PtCl_4/0.9% HCl(aq) for 1 h, (b) 1 mM Na_2PtCl_4/0.9% HCl(aq) for 1 h, (c) 10 mM Na_2PtCl_4/0.9% HCl(aq) for 1 h, (d) 0.1 mM Na_2PtCl_4/0.9% HCl(aq) for 3 h, (e) 1 mM Na_2PtCl_4/0.9% HCl(aq) for 3 h, and (f) 10 mM Na_2PtCl_4/0.9% HCl(aq) for 3 h, followed by oxygen plasma treatment in all cases.

information about the height and uniformity of the resulting platinum lines. The results of the SEM and AFM characterization of different [$Na_2(PtCl_4)$] and immersion times are summarized graphically in Figure 5; the width of the Pt features was determined by SEM and the height by AFM. The maximum width of the wires varies from ~7 to ~12 nm, which is about 3 nm smaller than their corresponding height.

The necessity for an accompanying acid source during the metal ion immersion step is demonstrated in Figure 6. SEM images and AFM surface plots of the platinum pattern formed after immersion in a solution of 10 mM $Na_2[PtCl_4]$(aq) for an extended time of 24 h shows that such treatment leads to only sparse platinum deposition (Figure 6a,b). Keeping time constant, increasing the concentration of HCl(aq) results in increased metal deposition going from 0.009% HCl(aq) to 9.0% HCl(aq). A hydrochloric acid concentration of 0.9% HCl(aq) (Figure 1a) is the lower limit that leads to complete platinum linear patterns over the entire surface of the block copolymer template-covered silicon surface; 0.09% HCl(aq), an acid concentration an order of magnitude less, at the standard 3 h immersion time, does not yield complete pattern transfer (Figure 6e,f). Division of the acid treatment and metal ion loading into two separate steps is also successful: pretreatment of the PS-P2VP monolayer with 1.0% HCl(aq), followed by rinsing with water and then immersion in a 10 mM $Na_2[PtCl_4]$(aq) solution for 3 h and plasma treatment, results in deposition of platinum lines (Supporting Information). Subtle differences in the resulting platinum morphology are observed (*i.e.*, more obvious formation of nodules down the length of the platinum line), but the approach is feasible.

Similar metallic lines are obtained on silicon using other anionic metal complexes based upon gold, palladium, iron, and cobalt; the metallic precursors utilized were $HAuCl_4$ or $KAuCl_4$ and Na_2PdCl_4, $K_3Fe(CN)_6$, and $K_3Co(CN)_6$, in the presence of HCl(aq), as shown in Figure 7. Cationic salts such as $AgNO_3$ [$Ag(H_2O)^+$(aq)] do not result in any observable metal deposition, certainly due to electrostatic repulsion between the protonated P2VP block and the positive charge on the metal ion (*vide infra*). Successful deposition of copper and nickel linear features was achieved from $CuCl_2$ and $NiCl_2$ in HF(aq), presumably due to *in situ* formation of anionic complexes such as $[CuX_4]^{2-}$, $[NiX_3]^-$, and $[NiX_4]^{2-}$ (X = Cl, F) under these conditions.[114–116] Subsequent plasma reduction produces pure metallic lines, as indicated by the X-ray photoelectron spectroscopy (XPS) results (Supporting Information).

Alignment *via* Graphoepitaxy. On flat, featureless substrates, the block copolymers self-assemble into horizontal fingerprint structures that lack long-range alignment and order, as shown in Figures 1−7. In order to effectively utilize the self-assembled block copolymer templates as interconnects, they must be aligned and directionally controlled. Using topologically defined silicon substrates, as outlined in Scheme 2, aligned self-assembly of a monolayer of the horizontal cylinders occurs within the 30–35-nm-deep trenches. This approach, an example of graphoepitaxy, has been well

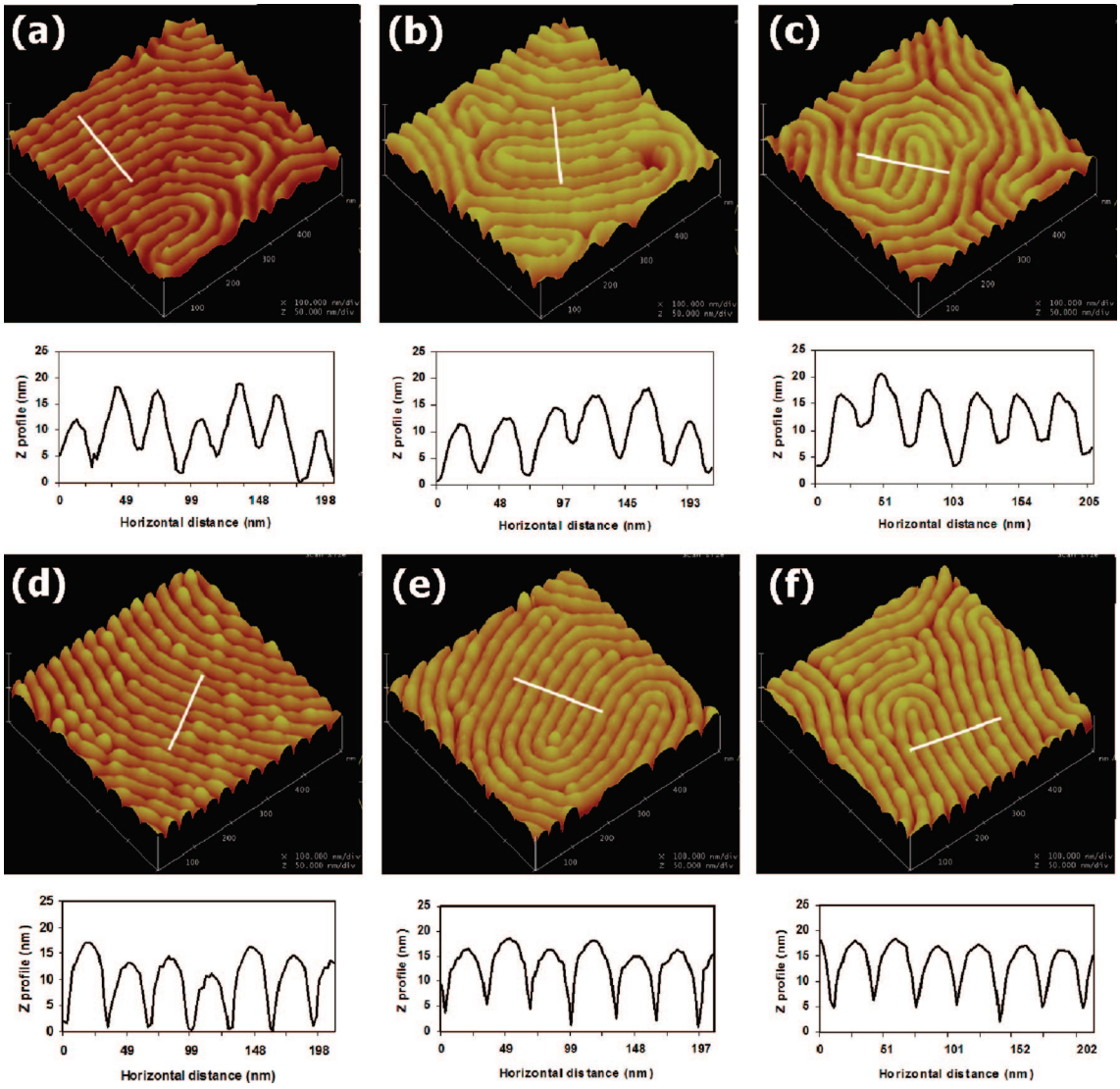

Figure 4. AFM images of the structures analyzed by SEM in Figure 3: (a) 0.1 mM Na_2PtCl_4/0.9% HCl(aq) for 1 h, (b) 1 mM Na_2PtCl_4/0.9% HCl(aq) for 1 h, (c) 10 mM Na_2PtCl_4/0.9% HCl(aq) for 1 h, (d) 0.1 mM Na_2PtCl_4/0.9% HCl(aq) for 3 h, (e) 1 mM Na_2PtCl_4/0.9% HCl(aq) for 3 h, and (f) 10 mM Na_2PtCl_4/0.9% HCl(aq) for 3 h, followed by oxygen plasma treatment.

demonstrated to produce controlled, directional nanoscale self-assembly of cylindrical phase block copolymers through microscale geometric substrate anisotropy, induced within confined spaces on flat interfaces.[117–126] High aspect ratio, parallel arrays of horizontal cylinders (sub-50 nm spacing, tens of micrometers long) can be easily accessed in this way. Immersion of the interfaces of the annealed, graphoepitxially defined block copolymer templates in a 10 mM Na_2PtCl_4/0.9% HCl(aq) solution for 3 h, followed by plasma reduction, resulted in aligned platinum lines, as shown in Figure 8. This method is effective for various shapes of predefined microdomains. For instance, Figures 8a shows ~10-nm-wide platinum lines aligned parallel to the surface in a 50-μm-long rectangular channel with a width of 400 nm. Other shapes can also result in aligned block copolymer assembly, including a triangular trench with a side length of 600 nm (Figure 8b) and 1-μm-diameter circular trenches (Figure 8c,d). A "yin-yang" assembly of the resulting platinum pattern ob-

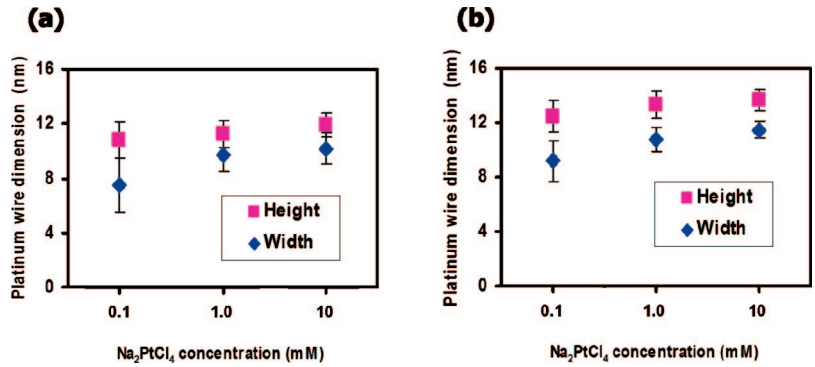

Figure 5. Summary of the height and width distribution of platinum nanowires formed under different deposition conditions. Depositions were carried out in 0.9% HCl(aq) and Na_2PtCl_4 solutions, with concentrations ranging from 0.1 to 10 mM for (a) 1 h and (b) 3 h.

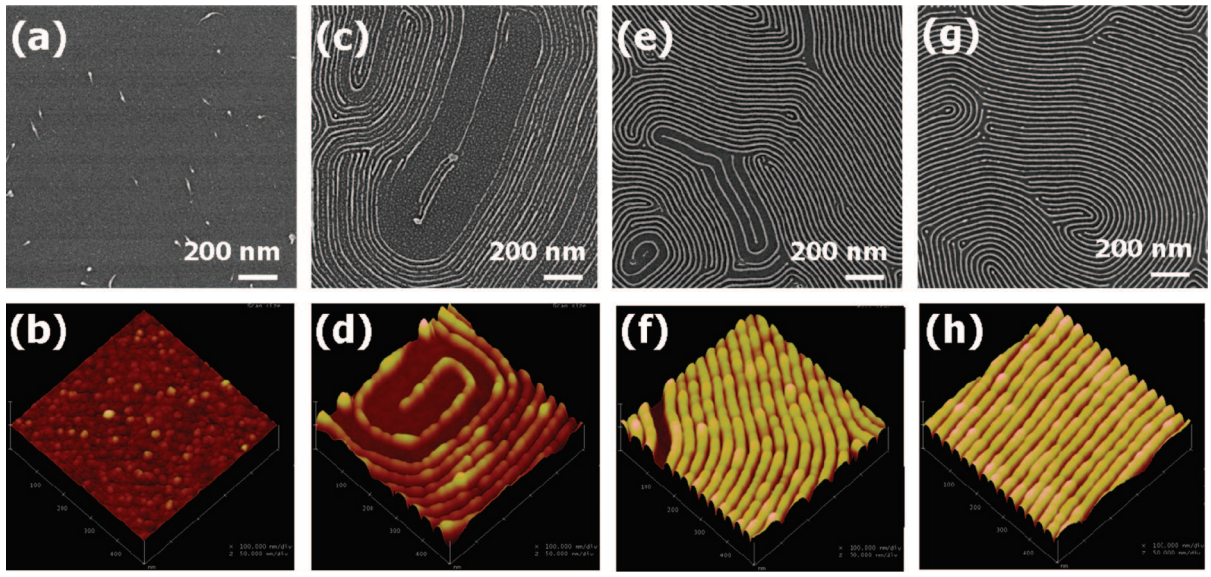

Figure 6. Platinum pattern transfer with different HCl(aq) concentrations. SEM images and AFM surface plots of platinum pattern transfer from the parent polymer film *via* deposition in an aqueous solution of 10 mM Na_2PtCl_4 (a,b) without HCl(aq) for 24 h, (c,d) with 0.009% HCl(aq) for 3 h, (e,f) with 0.09% HCl(aq) for 3 h, and (g,h) with 9% HCl(aq) for 3 h, followed by plasma treatment in all cases.

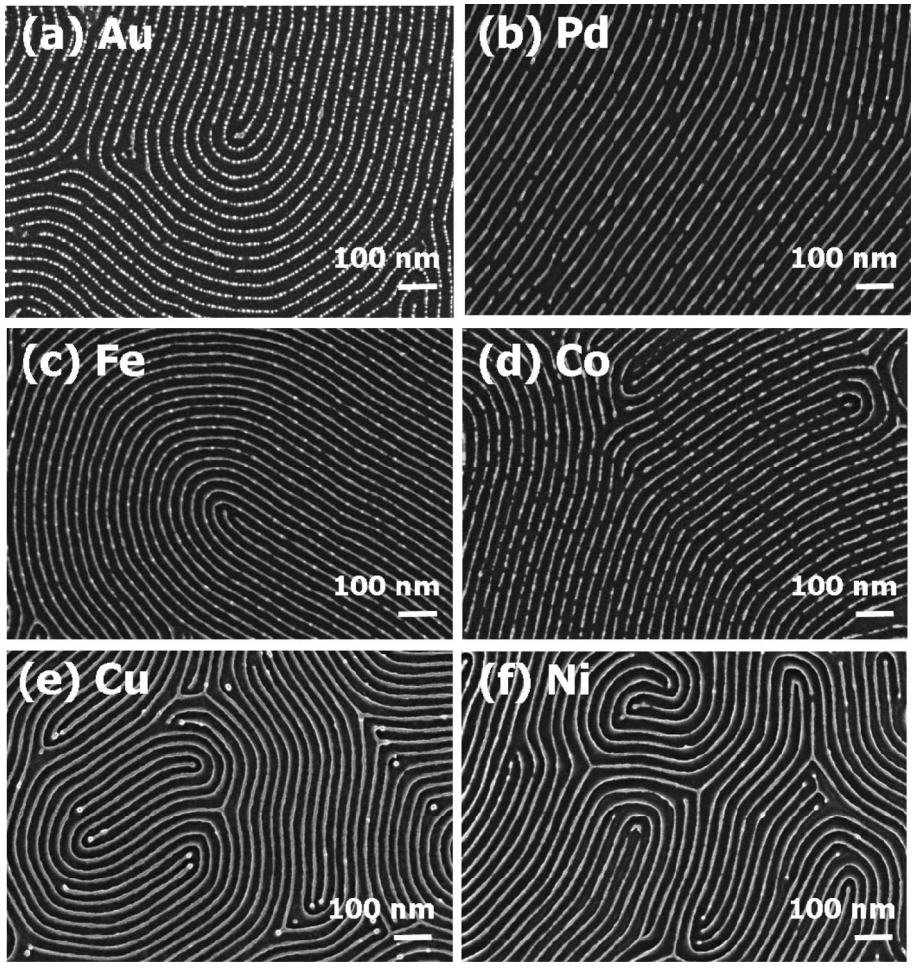

Figure 7. Patterning of different metals on silicon. SEM images of different metallic lines of different compositions: (a) Au, obtained by deposition in 10 mM $HAuCl_4$/0.9% HCl(aq) for 3 h; (b) Pd, obtained by deposition in 10 mM $Na_2[PdCl_4]$/0.9% HCl(aq) for 3 h; (c) Fe, obtained by deposition in 10 mM $K_3Fe(CN)_6$/0.9% HCl(aq) for 3 h; (d) Co, obtained by deposition in 10 mM $K_3Co(CN)_6$/0.9% HCl(aq) for 3 h; (e) Cu, obtained by deposition in 10 mM $CuCl_2$/0.9% HF(aq) for 15 min; and (f) Ni, obtained by deposition in 10 mM $NiCl_2$/0.9% HF(aq) for 15 m, followed by oxygen plasma treatment.

served in Figure 8d can be reproducibly induced through the introduction of a small defect in the topmost edge of the circular trench (highlighted with an arrow), resulting in misalignment throughout the self-assembled structure. In this manner, a broad array of interesting metallic patterns for different functions can be prepared. Micrometer-scale lithographic definition of features on silicon is straightforward and simple, whereas nanoscale lithography is considerably more difficult; the integration of the two length scales in this manner means that self-assembly can address the more challenging nanoscale patterning aspects, within a larger region well defined *via* standard and efficient lithographic procedures. While e-beam lithography was used here, scale-up using standard photolithography would be easily attainable.

Mechanism of Block Copolymer Loading with Metal Ions. Empirical screening of a variety of synthetic conditions led to the conclusion that an acidic, aqueous immersion is required for metal

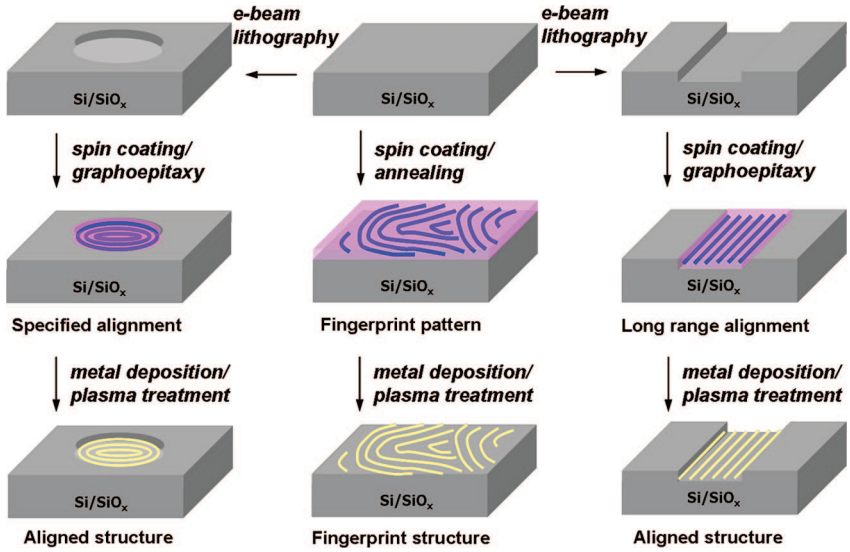

Scheme 2. Schema outlining alignment of self-assembled metallic nanowires *via* graphoepitaxy. Spin coating of the PS-P2VP polymer solution on a Si surface with trenches or other specified geometries, followed by thermal annealing, leads to self-assembly within a confined area, producing long-range alignment of metallic nanostructures.

ion loading, and that the metal ions must have a net negative charge. As shown in the AFM image in Figure 9a, the monolayer of thermally annealed PS-*b*-P2VP is flat and featureless on the nanometer scale, as the P2VP cylinders are buried within a uniform layer of polystyrene developed as the equilibrium morphology.[127,128] The polystyrene block forms a hydrophobic barrier between the P2VP core and the aqueous solution, precluding efficient contact between the metal ions in solution and the P2VP block which is to be loaded. In the presence of dilute acid, 0.01% HCl(aq), however, the effect of acid on the block coplymer structure can be observed *via* AFM; dilute acid serves to slow down the process to better image the resulting morphological shift. The AFM images in Figure 9 (also available as a movie), taken in fluid *via* tapping mode, approximately 10 min apart, reveal the gradual appearance of the protonated P2VP blocks, through the flat PS layer, and appearance of indentations in the center of the protonated P2VP features toward the end of this time. After ~2.5 h at this low HCl(aq) concentration, the nanoscale pattern of the P2VP template is fully exposed through the PS. The hydrodynamic diameter of the P2VP block of PS-*b*-P2VP block copolymers and microgels in aqueous solution is well established to increase several-fold upon protonation at a pH $<$ 4.5.[129,130] In this case of the block copolymer monolayer on the silicon surface, swelling forces the cationic P2VP to pierce and penetrate the PS overlayer, thus making direct contact with aqueous solution. The equilibrium chain conformation is a balance between the electrostatic interaction of the charged pyridyl cationic groups, which favor stretching, and the conformational entropy of the P2VP chains, which opposes stretching. The volume expansion of the P2VP domains results in the rupture of the PS corona toward the film's free surface, as indicated in Scheme 3. Upon further exposure to acid, the P2VP cylinders are constrained by the surrounding glassy PS matrix from swelling laterally underneath the film/solution interface and forced to swell above the ruptured area of PS to form mushroom-like caps. This self-associated behavior is similar to that of poly(styrene-*block*-acrylic acid) (PS-*b*-PAA) in an alkaline solution, where the film morphology differs by the degree of swelling depending upon the pH of the aqueous solution.[131–133] As shown in Figure 10, the formation of extruded cylinders appears more favorable in solutions of higher acidity, based on surface mor-

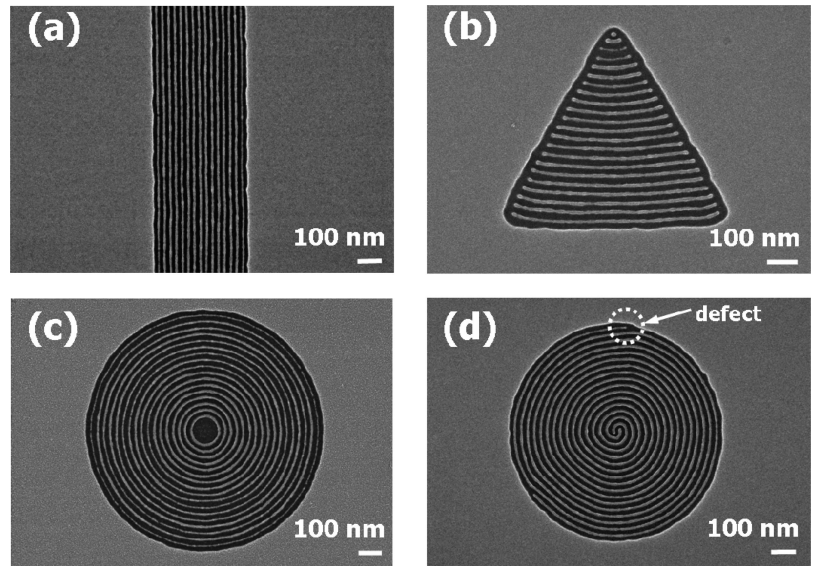

Figure 8. Aligned platinum nanostructures with long-range order. SEM images of platinum nanowires aligned within the ~35-nm-deep trenches on silicon: (a) rectangular channel with a width of 400 nm, (b) triangular trench with a side length of 600 nm, (c) circle with a diameter of 1 μm, and (d) circle with a radius of 400 nm ("yin-yang" shaped lines are formed due to edge defects). In all cases, structures were formed after deposition in 10 mM Na_2PtCl_4/0.9% HCl(aq) for 3 h, followed by oxygen plasma treatment.

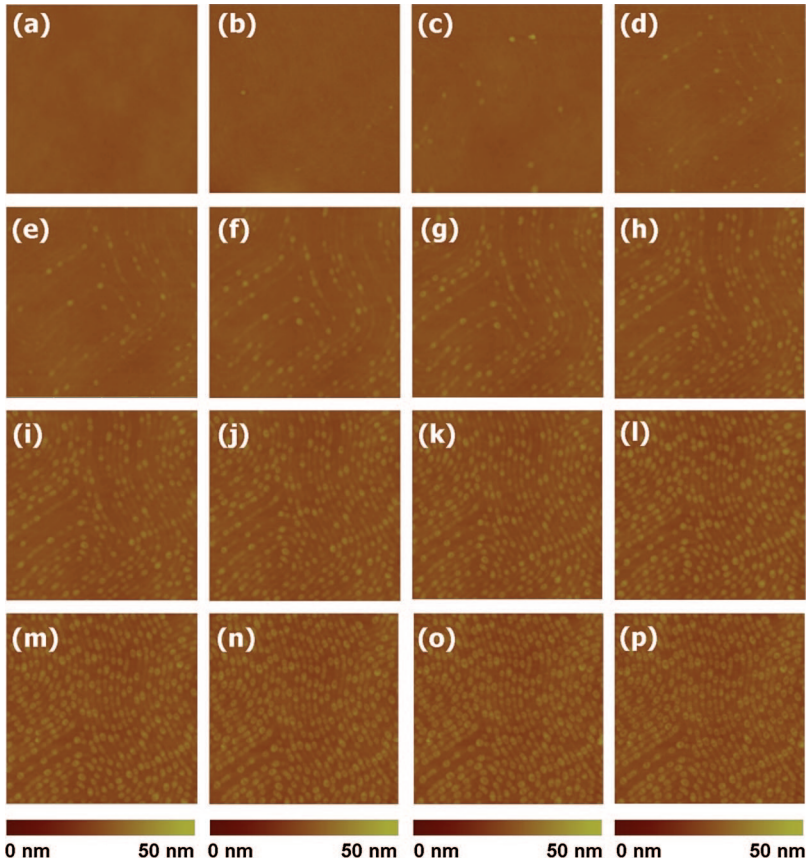

Figure 9. *In situ* AFM fluid cell observation of annealed PS-*b*-P2VP in acid. Morphological evolution of annealed PS(32500)-*b*-P2VP(12000) in 0.01% HCl(aq) for 0 to ~2.5 h for (a) 0 (prior to HCl(aq) treatment), (b) 10, (c) 20, (d) 30, (e) 40, (f) 50, (g) 60, (h) 70, (i) 80, (j) 90, (k) 100, (l) 110, (m) 120, (n) 130, (o) 140, and (p) 150 min.

Ⓦ A movie, in AVI format, showing the evolution of PS-*b*-P2VP morphology in acid is available.

phology comparison by AFM through a range of the HCl concentrations from 0.1% to 1% and 10%(aq). After soaking in the 0.1% and 1% HCl(aq) solution for 10 min, only a fraction of the protonated P2VP block is observed at the interface (Figure 10a,b), whereas the entire surface is covered by swollen P2VP cylinders in 10% HCl(aq) for the same soaking time, 10 min (Figure 10c). When the immersion time increases to 1 h, all the embedded P2VP chains swell to the surface in 1% and 10% HCl(aq), as shown in Figure 10e,f; the protonation of P2VP was not fully completed in 0.1% HCl(aq) after even a 1 h immersion (Figure 10d).

The loading of the block copolymer nanostructures can be easily understood as a protonation of the P2VP block, most likely *via* passage of hydronium ion that diffuses through the overlying PS layer. Protonation of the P2VP layer results in a large volume expansion of this block that then pierces the featureless polystyrene, making contact with the overlying aqueous layer. Anionic metal ion complexes are required for loading into the P2VP block, since it is positively charged. Electrostatic attraction between the anionic metal salt and the cationic P2VP block (again, in contact with the aqueous solution) leads to effective loading with the desired metal anion. A brief plasma treatment results in simultaneous metal ion reduction and block copolymer destruction and removal, leading to formation of the resulting metal lines on the surface. The entire process, from the spin coating of polymer solution to the formation of metallic nanowires, is summarized in Figure S3, Supporting Information. While the size of the P2VP micelles increases after acid treatment due to the swelling, and the width of the Pt lines decreases after plasma reduction, the center-to-center spacing of the P2VP cylinders does not vary after thermal annealing.

CONCLUSIONS

The self-assembled template material described here, the block copolymer, brings chemical selectivity, functionality, and the diversity of synthetic organic chemistry to the inorganic medium of semiconductor surface science. Through modulation of the processing parameters (deposition time, acidic strength, metallic ion concentration, molecular weight of block copolymers, *etc.*), the periodicity, size, morphology, and composition of the resulting metallic nanopatterns can be controlled. The acid-responsive nature of the block copolymer is key to success of the wet chemistry approach with respect to loading of the various metal ions. The synergy of the combination of bottom-up and top-down approaches to produce ordered linear metallic nanostructures *via* graphoepitaxy has enormous potential to integrate both soft materials with a range of hard, technologically important semiconductors, as well as micro- and nanoscales.

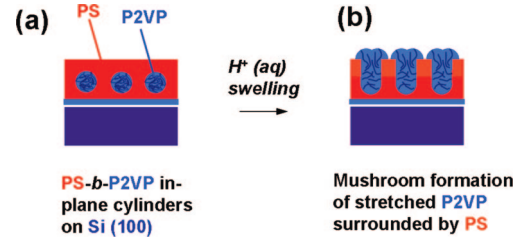

Scheme 3. Schematic illustration of the acid-reponsive behavior of PS-*b*-P2VP nanostructured films. (a) Cross-sectional view of thermally annealed PS-*b*-P2VP thin films with P2VP cylinders oriented in a parallel fashion to the surface, embedded in a PS matrix on a SiO_x substrate. (b) The proton-responsive P2VP block swells upon acid exposure, leading to direct contact with the aqueous solution.

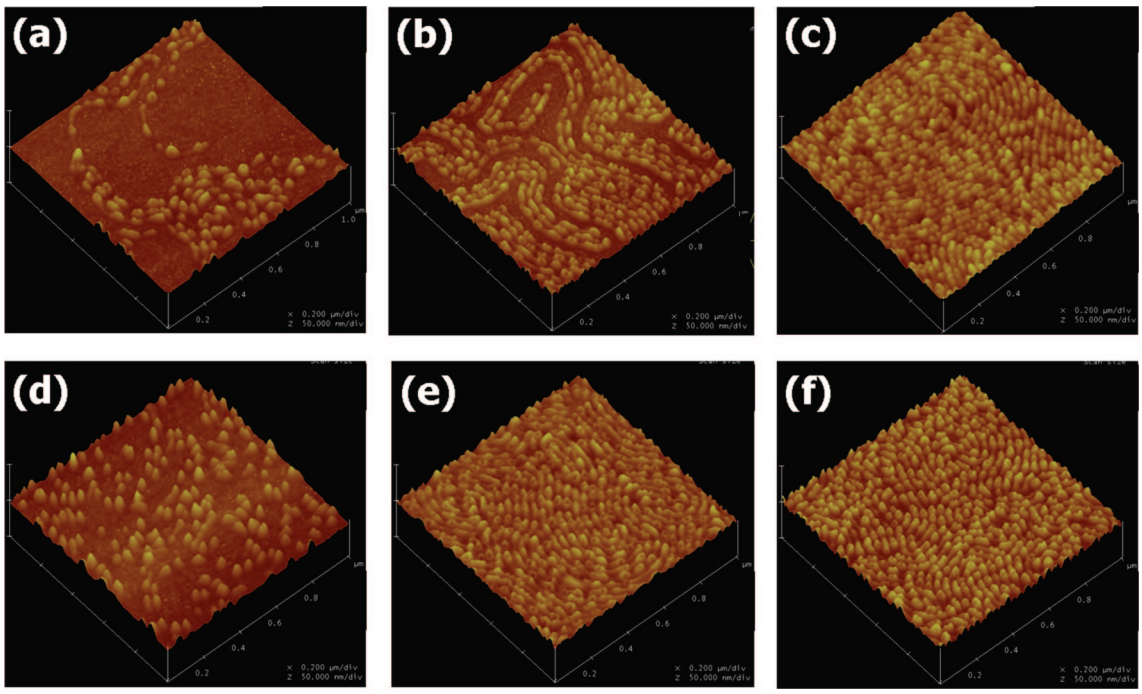

Figure 10. AFM images showing the response of the PS-*b*-P2VP block copolymer films to acid. Tapping-mode AFM surface plots of annealed PS-*b*-P2VP thin film monolayers on SiO_x after exposure to HCl(aq) concentrations of (a) 0.1% for 10 min, (b) 1% for 10 min, (c) 10% for 10 min, (d) 0.1% for 1 h, (e) 1% for 1 h, and (f) 10% for 1 h.

METHODS

Generalities. All the experiments were performed under ambient conditions at room temperature unless otherwise noted. Si(100) (n-type, B-doped, $\rho = 0.01–0.02\ \Omega \cdot cm$) wafers were purchased from Addison Engineering. $HAuCl_4$ (99.9995%) was purchased from Sigma-Aldrich, and $CuCl_2 \cdot 2H_2O$, $NiCl_2 \cdot 6H_2O$, $Na_2PtCl_4 \cdot xH_2O$, $Na_2PdCl_4 \cdot 3H_2O$, $K_3Fe(CN)_6$, and $K_3Co(CN)_6$ were acquired from Strem Chemicals. Water was obtained from a Millipore system (resistivity $> 18\ M \cdot \Omega$). Toluene was HPLC grade (Sigma-Aldrich), and methanol was Optima grade (Fisher). All reagents listed above were used without further purification. Teflon beakers and tweezers were used exclusively during the cleaning and preparation of the Si wafers and for all metal deposition procedures.

Silicon Cleaning Procedures. Si(100) wafers were diced into ~1 cm^2 pieces and degreased in a methanol ultrasonic bath for 15 min, followed by drying in a nitrogen stream. The substrates were then cleaned *via* a standard RCA clean:[112] the diced wafers were first immersed in a hot solution of $H_2O:NH_4OH:H_2O_2$ (5:1:1) for 15 min and then rinsed with copious excess Millipore water. They were then immersed in a hot $H_2O:HCl:H_2O_2$ (6:1:1) solution for 15 min. The wafers were again rinsed with excess Miilipore water. Following this cleaning procedure, the wafers were visibly hydrophilic; water on the surface was immediately removed with a stream of nitrogen before polymer spin coating.

Polymer Template Preparation. The asymmetric diblock copolymers, polystyrene-*block*-poly(2-vinylpyridine) (PS-*b*-P2VP) with different molecular weights, were purchased from Polymer Source Inc. (www.polymersource.com, Dorval, Quebec, Canada). They were used without purification. The polymers were dissolved in toluene at 70 °C to make a ~1% w/w solution and allowed to cool to room temperature. A 10 μL sample of the polymer solution was then dropped onto a 1 cm^2 Si wafer and spin coated (spin coater model WS-400B-6NPP-Lite, Laurell Technologies, North Wales, PA) in an inert environment. The thickness of the thin films was controlled by modifying the solution concentration and spin speed. Subsequent thermal annealing of the samples was carried out at 230 °C under vacuum for 24 h.

Metal Deposition. The polymer-coated wafer was immersed in the desired aqueous metal salt solution (with or without HCl/HF) held in a Teflon beaker. The metal salt solutions were prepared by mixing the metal salt solution and HCl(aq) or HF(aq) of the desired concentration for a given time. After metal deposition, the sample was thoroughly rinsed with water and dried under a nitrogen stream. Oxygen plasma was generally employed to remove the polymer and reduce the metal ions. The thin layer of oxide on the metallic film can be removed by a brief argon plasma sputtering.

Trench Fabrication on Silicon. Diced silicon wafers (1 cm^2) were spin coated with poly(methyl methacrylate) (MW 950000) and baked at 180 °C for 2 min. Rectangular, triangular, and circular trenches with varying dimensions were then fabricated by electron beam ligthography (EBL) using a Raith 150 system, followed by SF_6 reactive ion etching. EBL was performed at an acceleration voltage of 10 kV and a dose of 300 pC/cm^2 to etch the troughs to a depth of ~35 nm.

Surface Characterization. Block copolymer and metal nanostructures on silicon were characterized by atomic force microscopy (AFM), scanning electron microscopy (SEM), scanning Auger microscopy (SAM), and X-ray photoelectron spectroscopy (XPS). SEM, SAM, and XPS were performed under high-vacuum conditions ($<10^{-8}$ Torr). The AFM used in this study was a Nanoscope IV (Digital Instruments/Veeco) using commercial Si cantilevers in tapping mode under ambient conditions. NSC18/AIBS (MikroMasch) probes were used to investigate polymer nanostructure evolution in acid in fluid tapping mode, whereas SSS-NCHR-50 (Nanosensors) probes with a 2 nm radius of curvature were used for other AFM characterizations. XPS high-resolution spectra were acquired with a Kratos Axis 165 photoelectron spectrometer using a monochromatic aluminum X-ray source (Al Kα 1486.6 eV) operating at 210 W (15 kV, 14 mA). The instrument was calibrated to the $4f_{7/2}$ peak of gold at $E_b = 84.0$ eV. Charge compensation was accomplished using low-energy electrons. Standard operating conditions for good charge compensation are –2.8 V bias voltage, −1.0 V filament voltage, and filament current of 2.1 A. Binding energies (BEs) were determined by reference to C 1s at BE of 284.6 eV. SAM (JEOL, JAMP-9500F) was carried out with an electron accelerating voltage and emission current of 25 kV and 10 nA, respectively. The Auger peaks of Pt

NVV (59 eV) were selected for the mapping. The Auger mapping for each element was obtained by plotting $(P - B)/B$, where P and B are peak and background intensities, respectively.

Acknowledgment. This work was supported by the National Research Council (NRC) of Canada, the University of Alberta, NSERC, and the Canadian Foundation for Innovation. J.C. acknowledges financial support from the Alberta Ingenuity studentship fund, a Killiam Memorial Scholarship, and an NSERC PGS-D scholarship. We are also thankful for the technical support provided at NINT, the Alberta Centre for Surface Engineering and Science (ACSES), and the Nanofab at the University of Alberta.

Supporting Information Available: Figure S1, XPS spectra of gold, palladium, iron, cobalt, copper, and nickel deposition on silicon; Figure S2, platinum pattern transfer after preloading of polymer monolayer with HCl(aq); and Figure S3, AFM height images showing PS-*b*-P2VP block copolymer/metal phase at various stages of processing. This information is available free of charge *via* the Internet at http://pubs.acs.org.

REFERENCES AND NOTES

1. Rosi, N. L.; Mirkin, C. A. Nanostructures in Biodiagnostics. *Chem. Rev.* **2005**, *105*, 1547–1562.
2. Link, S.; El-Sayed, M. A. Optical Properties and Ultrafast Dynamics of Metallic Nanocrysals. *Annu. Rev. Phys. Chem.* **2003**, *54*, 331–66.
3. DeVries, G. A.; Brunnbauer, M.; Hu, Y.; Jackson, A. M.; Long, B.; Neltner, B. T.; Uzun, O.; Wunsch, B. H.; Stellacci, F. Divalent Metal Nanoparticles. *Science* **2007**, *315*, 358–361.
4. Soong, R. K.; Bachand, G. D.; Neves, H. P.; Olkhovets, A. G.; Craighead, H. G.; Montemagno, C. D. Powering an Inorganic Nanodevice with a Biomolecular Motor. *Science* **2000**, *290*, 1555–1558.
5. Nelayah, J.; Kociak, M.; Stéphan, O.; García de Abajo, F. J.; Tencé, M.; Henrard, L.; Taverna, D.; Pastoriza-Santos, I. M.; Liz-Marzán, L.; Colliex, C. Mapping Surface Plasmons on a Single Metallic Nanoparticle. *Nat. Phys.* **2007**, *3*, 348–353.
6. Javey, A.; Dai, H. J. Regular Arrays of 2 nm Metal Nanoparticles for Deterministic Synthesis of Nanomaterials. *J. Am. Chem. Soc.* **2003**, *127*, 11942–11943.
7. Wiley, B. J.; Chen, Y. C.; McLellan, J. M.; Xiong, Y. J.; Li, Z. Y.; Ginger, D.; Xia, Y. N. Synthesis and Optical Properties of Silver Nanobars and Nanorice. *Nano Lett.* **2007**, *7*, 1032–1036.
8. Pundt, A.; Kirchheim, R. Hydrogen in Metals: Microstructural Aspects. *Annu. Rev. Mater. Res.* **2006**, *36*, 555–608.
9. Michaels, A. M.; Nirmal, M.; Brus, L. E. Surface Enhanced Raman Spectroscopy of Individual Rhodamine 6G Molecules on Large Ag Nanocrystals. *J. Am. Chem. Soc.* **1999**, *121*, 9932–9939.
10. Choi, H. S.; Liu, W.; Misra, P.; Tanaka, E.; Zimmer, J. P.; Kandapallil, B.; Bawendi, M. G.; Frangioni, J. V. Renal Clearance of Nanoparticles. *Nat. Biotechnol.* **2007**, *25*, 1165–1170.
11. Terabe, K.; Hasegawa, T.; Nakayama, T.; Aono, M. Quantized Conductance Atomic Switch. *Nature* **2005**, *433*, 47–50.
12. Schmid, G.; Chi, L. F. Metal Clusters and Colloids. *Adv. Mater.* **1998**, *10*, 515–526.
13. Xia, Y. N.; Yang, P. D.; Sun, Y.; Wu, Y.; Mayers, B.; Gates, B.; Yin, Y.; Kim, F.; Yan, H. One-Dimensional Nanostructures: Synthesis, Characterization, and Applications. *Adv. Mater.* **2003**, *15*, 353–389.
14. Wang, Z. L., Ed. *Nanowires and Nanobelts—Materials, Properties and Devices*; Klumer Academic Publishers: Boston, 2003.
15. Kline, T. R.; Tian, M.; Wang, J.; Sen, Y.; Chan, M. W. H.; Mallouk, T. E. Template-Grown Metal Nanowires. *Inorg. Chem.* **2006**, *45*, 7555–7565.
16. Wu, Y.; Xiang, J.; Yang, C.; Lu, W.; Lieber, C. M. Single-Crystal Metallic Nanowires and Metal/Semiconductor Nanowire Heterostructures. *Nature* **2004**, *430*, 61–65.
17. Ieong, M.; Doris, B.; Kedzierski, J.; Rim, K.; Yang, M. Silicon Device Scaling to the Sub-10-nm Regime. *Science* **2004**, *306*, 2057–2060.
18. Chen, J. Y.; Wiley, B. J.; Xia, Y. N. One-Dimensional Nanostructures of Metals: Large-Scale Synthesis and Some Potential Applications. *Langmuir* **2007**, *23*, 4120–4129.
19. Knight, M. W.; Grady, N. K.; Bardhan, R.; Hao, F.; Nordlander, P.; Halas, N. J. Nanoparticle-Mediated Coupling of Light into a Nanowire. *Nano Lett.* **2007**, *7*, 2346–2350.
20. Wei, Z. Q.; Zamborini, F. P. Directly Monitoring the Growth of Gold Nanoparticle Seeds into Gold Nanorods. *Langmuir* **2004**, *20*, 11301–11304.
21. Yaliraki, S. N.; Kemp, M.; Ratner, M. A. Conductance of Molecular Wires: Influence of Molecule-Electrode Binding. *J. Am. Chem. Soc.* **1999**, *121*, 3428–3434.
22. Orendorff, C. J.; Baxter, S. C.; Goldsmith, E. C.; Murphy, C. J. Light Scattering from Gold Nanorods: Tracking Material Deformation. *Nanotechnology* **2005**, *16*, 2601–2605.
23. Xu, Q.; Bao, J.; Capasso, F.; Whitesides, G. M. Surface Plasmon Resonances of Free-Standing Gold Nanowires Fabricated by Nanoskiving. *Angew. Chem., Int. Ed.* **2006**, *45*, 3631–3635.
24. Soennichsen, C.; Alivisatos, A. P. Gold Nanorods as Novel Nonbleaching Plasmon-Based Orientation Sensors for Polarized Single-Particle Microscopy. *Nano Lett.* **2005**, *5*, 301–304.
25. Melosh, N. A.; Boukai, A.; Diana, F.; Gerardot, B.; Badolato, A.; Petroff, P. M.; Heath, J. R. Ultrahigh-Density Nanowire Lattice and Circuits. *Science* **2003**, *300*, 112–115.
26. Salaita, K.; Wang, Y.; Mirkin, C. A. Applications of Dip-Pen Nanolithography. *Nat. Nanotechnol.* **2007**, *2*, 145–155.
27. Craighead, H. G. Nanoelectromechanical Systems. *Science* **2000**, *290*, 1532–1535.
28. Storm, A. J.; Chen, J. H.; Ling, X. S.; Zandbergen, H. W.; Dekker, C. Fabrication of Solid-State Nanopores with Single Nanometer Precision. *Nat. Mater.* **2003**, *2*, 537–540.
29. Seal, S.; Kuiry, S. C.; Georgieva, R.; Agarwal, A. Manufacturing Nancomposite Parts: Present Status and Future Challenges. *MRS Bull.* **2004**, *29*, 16–21.
30. Ginger, D. S.; Zhang, H.; Mirkin, C. A. The Evolution of Dip-pen Nanolithography. *Angew, Chem., Int. Ed.* **2004**, *43*, 30–45.
31. Park, H.; Lim, A. K. L.; Alivisatos, A. P.; Park, J.; McEuen, P. L. Fabrication of Metallic Electrodes with Nanometer Separation by Electromigration. *Appl. Phys. Lett.* **1999**, *75*, 301–303.
32. Xu, L.; Vemula, S. C.; Jain, M.; Nam, S. K.; Donnelly, V. M.; Economou, D. J.; Ruchhoeft, P. Nanopantography: A New Method for Massively Parallel Nanopatterning over Large Areas. *Nano Lett.* **2005**, *5*, 2563–2568.
33. Gates, B. D.; Xu, Q. B.; Stewart, M.; Ryan, D.; Willson, C. G.; Whitesides, G. M. New Approaches to Nanofabrication: Molding, Printing, and Other Techniques. *Chem. Rev.* **2005**, *105*, 1171–1196.
34. Bratton, D.; Yang, D.; Dai, J. Y.; Ober, C. K. Recent Progress in High Resolution Lithography. *Polym. Adv. Technol.* **2006**, *17*, 94–103.
35. Mullen, T. J.; Srinivasan, C.; Hohman, J. N.; Gillmor, S. D.; Shuster, M. J.; Horn, M. W.; Andrews, A. M.; Weiss, P. S. Microcontact Insertion Printing. *Appl. Phys. Lett.* **2007**, *90*, 063114.
36. Geissler, M.; Xia, Y. N. Patterning: Principles and Some New Developments. *Adv. Mater.* **2004**, *16*, 1249–1269.
37. Chou, S. Y.; Keimel, C.; Gu, J. Ultrafast and Direct Imprint of Nanostructures in Silicon. *Nature* **2002**, *417*, 835–837.
38. ITRS. *International Technology Roadmap for Semiconductors 2006 Update*; http://www.itrs.net (under "Reports").
39. Huber, C. A.; Huber, T. E.; Sadoqi, M.; Lubin, J. A.; Manalis, S.; Prater, C. B. Nanowire Array Composites. *Science* **1994**, *263*, 800–802.
40. Crowley, T. A.; Ziegler, K. J.; Lyons, D. M.; Erts, D.; Olin, H.; Morris, M. A.; Holmes, J. D. Synthesis of Metal and Metal Oxide Nanowire and Nanotube Arrays within a

Mesoporous Silica Template. *Chem. Mater.* **2003**, *15*, 3518–3522.
41. Martin, C. R. Nanomaterials—A Membrane-Based Synthetic Approach. *Science* **1994**, *266*, 1961–1966.
42. Martin, B. R.; Dermody, D. J.; Reiss, B. D.; Fang, M. M.; Lyon, L. A.; Natan, M. J.; Mallouk, T. E. Orthogonal Self-Assembly on Colloidal Gold-Platinum Nanorods. *Adv. Mater.* **1999**, *11*, 1021–1025.
43. Huang, M. H.; Choudrey, A.; Yang, P. D. Ag Nanowire Formation within Mesoporous Silica. *Chem. Commun.* **2000**, *12*, 1063–1064.
44. Kijima, T.; Yoshimura, T.; Uota, M.; Ikeda, T.; Fujikawa, D.; Mouri, S.; Uoyama, S. Noble-Metal Nanotubes (Pt, Pd, Ag) from Lyotropic Mixed-Surfactant Liquid-Crystal Templates. *Angew. Chem., Int. Ed.* **2004**, *43*, 228–232.
45. Fullam, S.; Cottell, D.; Rensmo, H.; Fitzmaurice, D. Carbon Nanotube Templated Self-Assembly and Thermal Processing of Gold Nanowires. *Adv. Mater.* **2000**, *12*, 1430–1432.
46. Mbindyo, J. K. N.; Reiss, B. D.; Martin, B. R.; Keating, C. D.; Natan, M. J.; Mallouk, T. E. DNA-Directed Assembly of Gold Nanowires on Complementary Surfaces. *Adv. Mater.* **2001**, *13*, 249–254.
47. Zach, M. P.; Ng, K. H.; Penner, R. M. Molybdenum Nanowires by Electrodeposition. *Science* **2000**, *290*, 2120–2123.
48. Menke, E. J.; Thompson, M. A.; Xiang, C.; Yang, L. C.; Penner, R. M. Lithographically Patterned Nanowire Electrodeposition. *Nat. Mater.* **2006**, *5*, 914–919.
49. Murray, B. J.; Walter, E. C.; Penner, R. M. Amine Vapor Sensing with Silver Mesowires. *Nano Lett.* **2004**, *4*, 665–670.
50. Penner, R. M. Mesoscopic Metal Particles and Wires by Electrodeposition. *J. Phys. Chem. B* **2002**, *106*, 3339–3353.
51. Hamley, I. W. Nanostructure Fabrication Using Block Copolymers. *Nanotechnology* **2003**, *14*, R39–R54.
52. Hawker, C. J.; Russell, T. P. Block Copolymer Lithography: Merging "Bottom-Up" with "Top-Down" Processes. *MRS Bull.* **2005**, *30*, 952–966.
53. Ikkala, O.; Brinke, G. Functional Materials Based on Self-Assembly of Polymeric Supramolecules. *Science* **2002**, *295*, 2407–2409.
54. Segelman, R. A. Patterning with Block Copolymer Thin Films. *Mater. Sci. Eng., R* **2005**, *48*, 191–226.
55. Ryu, D. Y.; Shin, K.; Drockenmuller, E.; Hawker, C. J.; Russell, T. P. A Generalized Approach to the Modification of Solid Surfaces. *Science* **2005**, *308*, 236–239.
56. Ludwigs, S.; Böker, A.; Voronov, A.; Rehse, N.; Magerle, R.; Krausch, G. Self-Assembly of Functional Nanostructures from ABC Triblock Copolymers. *Nat. Mater.* **2005**, *2*, 744–747.
57. Glass, R.; Möller, M.; Spatz, J. Block Copolymer Micelle Nanolithography. *Nanotechnology* **2003**, *14*, 1153–1160.
58. Aizawa, M.; Buriak, J. M. Nanoscale Patterning of Two Metals on Silicon Surfaces Using an ABC Triblock Copolymer Template. *J. Am. Chem. Soc.* **2006**, *128*, 5877–5886.
59. Shenhar, R.; Jeoung, E.; Srivistava, S.; Norsten, T. B.; Rotello, V. M. Crosslinked Nanoparticle Stripes and Hexagonal Networks Obtained via Selective Patterning of Block Copolymer Thin Films. *Adv. Mater.* **2005**, *17*, 2206–2210.
60. Lopes, W. A.; Jaeger, H. M. Hierarchical Self-assembly of Metal Nanostructures on Diblock Copolymer Scaffolds. *Nature* **2001**, *414*, 735–738.
61. Cheng, J. Y.; Ross, C. A.; Chan, V. Z. H.; Thomas, E. L.; Lammertink, R. G. H.; Vancso, G. J. Formation of a Cobalt Magnetic Dot Array via Block Copolymer Lithography. *Adv. Mater.* **2001**, *13*, 1174–1178.
62. Ansari, I. A.; Hamley, I. W. Templating the Patterning of Gold Nanoparticles Using a Stained Triblock Copolymer Film Surface. *J. Mater. Chem.* **2003**, *13*, 2412–2413.
63. Park, M.; Chaikin, P. M.; Register, R. A.; Adamson, D. H. Large Area Dense Nanoscale Patterning of Arbitrary Surfaces. *Appl. Phys. Lett.* **2001**, *79*, 257–259.
64. Cheng, J. Y.; Jung, W.; Ross, C. A. Magnetic Nanostructures from Block Copolymer Lithography: Hysteresis, Thermal Stability, and Magnetoresistance. *Phys. Rev. B* **2004**, *70*, 064417.
65. Thurn-Albrecht, T.; Schotter, J.; Kastle, G. A.; Emley, N.; Shibauchi, T.; Krusin-Elbaum, L.; Guarini, K.; Black, C. T.; Tuominen, M. T.; Russell, T. P. Ultrahigh-Density Nanowire Arrays Grown in Self-Assembled Diblock Copolymer Templates. *Science* **2000**, *290*, 2126–2129.
66. Darling, S. B.; Yufa, N. A.; Cisse, A. L.; Bader, S. D.; Sibener, S. J. Self-Organization of FePt Nanoparticles on Photochemically Modified Diblock Copolymer Templates. *Adv. Mater.* **2005**, *17*, 2446–2450.
67. Meli, M.-V.; Badia, A.; Gruetter, P. & Lennox, R. B. Self-Assembled Masks for the Transfer of Nanometer-Scale Patterns into Surfaces: Characterization by AFM and LFM. *Nano Lett.* **2002**, *2*, 131–135.
68. Malenfant, P. R. L.; Wan, J.; Taylor, S. T. & Manoharan, M. Self-assembly of an organic–inorganic block copolymer for nano-ordered ceramics. *Nat. Nanotechnol.* **2007**, *2*, 43–46.
69. Braun, P. V.; Wiltzius, P. Microporous Materials—Electrochemically Grown Photonic Crystals. *Nature* **1999**, *402*, 603–604.
70. Bailey, R. C.; Stevenson, K. J.; Hupp, J. T. Assembly of Micropatterned Colloidal Gold Thin Films via Microtransfer Molding and Electrophoretic Deposition. *Adv. Mater.* **2000**, *12*, 1930–1934.
71. Hamley, I. W. Nanotechnology with Soft Materials. *Angew. Chem., Int. Ed.* **2003**, *42*, 1692–1712.
72. Ruzette, A.-V.; Leibler, L. Block Copolymers in Tomorrow's Plastics. *Nat. Mater.* **2005**, *4*, 19–31.
73. Ikkala, O.; Brinke, G. Hierarchical Self-Assembly in Polymeric Complexes: Towards Functional Materials. *Chem. Commun.* **2004**, *19*, 2131–2137.
74. Haryono, A.; Binder, W. H. Controlled Arrangement of Nanoparticle Arrays in Block-Copolymer Domains. *Small* **2006**, *2*, 600–611.
75. Bates, F. S.; Fredrickson, G. H. Block Copolymers—Designer Soft Materials. *Phys. Today* **1999**, *52*, 32–38.
76. Park, C.; Cheng, J. Y.; DeRosa, C.; Fasolka, M. J.; Mayes, A. M.; Ross, C. A.; Thomas, E. L. Double Textured Cylindrical Block Copolymer Domains via Directional Solidification on a Topographically Patterned Substrate. *Appl. Phys. Lett.* **2001**, *79*, 848–850.
77. Wang, X. S.; Guerin, G.; Wang, H.; Wang, Y. S.; Manners, I.; Winnik, M. A. Cylindrical Block Copolymer Micelles and Co-Micelles of Controlled Length and Architecture. *Science* **2007**, *317*, 644–647.
78. Antonietti, M.; Foerster, S.; Hartmann, J.; Oestreich, S. Novel Amphiphilic Block Copolymers by Polymer Reactions and Their Use for Solubilization of Metal Salts and Metal Colloids. *Macromolecules* **1996**, *29*, 3800–3806.
79. Albrecht, K.; Mourran, A.; Moller, M. Surface Micelles and Surface-Induced Nanopatterns Formed by Block Copolymers. *Adv. Polym. Sci.* **2006**, *200*, 57–70.
80. Cox, J. K.; Eisenberg, A.; Lennox, R. B. Patterned Surfaces via Self-Assembly. *Curr. Opin. Colloid Interface Sci.* **1999**, *4*, 52–59.
81. Krausch, G.; Magerle, R. Nanostructured Thin Films via Self-Assembly of Block Copolymers. *Adv. Mater.* **2002**, *14*, 1579–1583.
82. Spontak, R. J.; Alexandridis, P. Advances in Self-Ordering Macromolecules and Nanostructure Design. *Curr. Opin. Colloid Interface Sci.* **1999**, *4*, 140–146.
83. Chiu, J. J.; Kim, B. J.; Kramer, E. J.; Pine, D. J. Control of Nanoparticle Location in Block Copolymers. *J. Am. Chem. Soc.* **2005**, *127*, 5036–5037.
84. Tsutsumi, K.; Funaki, Y.; Hirokawa, Y.; Hashimoto, T. Selective Incorporation of Palladium Nanoparticles into Microphase-Separated Domains of Poly(2-vinylpyridine)-*block*-Polyisoprene. *Langmuir* **1999**, *15*, 5200–5203.
85. Minelli, C.; Hinderling, C.; Heinzelmann, H.; Pugin, R.; Liley, M. Micrometer-Long Nanowires Fabricated Using Block Copolymer Templates. *Langmuir* **2005**, *21*, 7080–7082.

86. Sohn, B. H.; Choi, J. M.; Yoo, S. I.; Yun, S. H.; Zin, W. C.; Jung, J. C.; Kanehara, M.; Hirata, T.; Teranishi, T. Directed Self-Assembly of Two Kinds of Nanoparticles Utilizing Monolayer Films of Diblock Copolymer Micelles. *J. Am. Chem. Soc.* **2003**, *125*, 6368–6369.
87. Grubbs, R. B. Roles of Polymer Ligands in Nanoparticle Stabilization. *Polym. Rev.* **2007**, *47*, 197–215.
88. Shenhar, R.; Jeoung, E.; Srivastava, S.; Norsten, T. B.; Rotello, V. M. Crosslinked Nanoparticle Stripes and Hexagonal Networks Obtained via Selective Patterning of Block Copolymer Thin Films. *Adv. Mater.* **2005**, *17*, 2206–2210.
89. Ciebien, J. F.; Clay, R. T.; Sohn, B. H.; Cohen, R. E. Brief review of metal nanoclusters in block copolymer films. *New J. Chem.* **1998**, *22*, 685–691.
90. Spatz, J. P. Nano- and Micropatterning by Organic-Inorganic Templating of Hierarchical Self-Assembled Structures. *Angew. Chem., Int. Ed.* **2002**, *41*, 3359–3362.
91. Li, M.; Ober, K. Block Copolymer Patterns and Templates. *Mater. Today* **2006**, *9*, 31–39.
92. Forster, S. Amphiphilic Block Copolymers for Templating Applications. *Top. Curr. Chem.* **2003**, *226*, 1–28.
93. Lazzari, M.; Lopez-Quintela, M. A. Block Copolymers as a Tool for Nanomaterial Fabrication. *Adv. Mater.* **2003**, *15*, 1583–1594.
94. Krishnamoorthy, S.; Hinderling, C.; Heinzelmann, H. Nanoscale Patterning with Block Copolymer. *Mater. Today* **2006**, *9*, 40–47.
95. Spatz, J. P.; Herzog, T.; Mossmer, S.; Ziemann, P.; Moller, M. Micellar Inorganic-Polymer Hybrid Systems—a Tool for Nanolithography. *Adv. Mater.* **1999**, *11*, 149–153.
96. Aizawa, M.; Buriak, J. M. Block Copolymer-Templated Chemistry on Si, Ge, InP, and GaAs Surfaces. *J. Am. Chem. Soc.* **2005**, *127*, 8932–8933.
97. Cuenya, B. R.; Baeck, S.-H.; Jaramillo, T. F.; McFarland, E. W. Size- and Support-Dependent Electronic and Catalytic Properties of Au^0/Au^{3+} Nanoparticles Synthesized from Block Copolymer Micelles. *J. Am. Chem. Soc.* **2003**, *125*, 12928–12934.
98. Bronstein, L. M.; Sidorov, S. N.; Zhirov, V.; Zhirov, D.; Kabachii, Y. A.; Kochev, S. Y.; Valetsky, P. M.; Stein, B.; Kiseleva, O. I.; Polyakov, S. N.; *et al.* Metalated Diblock and Triblock Poly(ethylene oxide)-block-poly(4-vinylpyridine) Copolymers: Understanding of Micelle and Bulk Structure. *J. Phys. Chem. B* **2005**, *109*, 18786–18798.
99. Sakai, T.; Alexandridis, P. Single-Step Synthesis and Stabilization of Metal Nanoparticles in Aqueous Pluronic Block Copolymer Solutions at Ambient Temperature. *Langmuir* **2004**, *20*, 8426–8430.
100. Sidorov, S. N.; Bronstein, L. M.; Kabachii, Y. A.; Valetshy, P. M.; Soo, P. L.; Maysinger, D.; Eisenberg, A. Influence of Metalation on the Morphologies of Poly(ethylene oxide)-*block*-poly(4-vinylpyridine) Block Copolymer Micelles. *Langmuir* **2004**, *20*, 3543–3550.
101. Spatz, J. P.; Roescher, A.; Moller, M. Gold Nanoparticles in Micellar Poly(styrene)-*b*-Poly(ethylene oxide) Films-Size and Interparticle Distance Control in Monoparticulate Films. *Adv. Mater.* **1996**, *8*, 337–340.
102. Abes, J. I.; Cohen, R. E.; Ross, C. A. Selective Growth of Cobalt Nanoclusters in Domains of Block Copolymer Films. *Chem. Mater.* **2003**, *15*, 1125–1131.
103. Tadd, E. H.; Bradley, J.; Tannenbaum, R. Spatial Distribution of Cobalt Nanoclusters in Block Copolymers. *Langmuir* **2002**, *18*, 2378–2384.
104. Deshmukh, R. D.; Buxton, G. A.; Clarke, N.; Composto, R. J. Nanoscale Block Copolymer Templates Decorated by Nanoparticle Arrays. *Macromolecules* **2007**, *40*, 6316–6324.
105. Fahmi, A. W.; Stamm, M. Spatially Correlated Metallic Nanostructures on Self-Assembled Diblock Copolymer Termplates. *Langmuir* **2005**, *21*, 1062–1066.
106. Clay, R. T.; Cohen, R. E. Synthesis of Metal Nanoclusters within Microphase-Separated Diblock Copolymers: Sodium Carboxylate vs Carboxylic Acid Functionalization. *Supramol. Sci.* **1998**, *5*, 41–48.
107. Yun, S. H.; Yoo, S. M.; Sohn, B. H.; Jung, J. C.; Zin, W. C.; Kwak, S. Y.; Lee, T. S. Electrically Anisotropic Thin Films Consisting of Polymeric and Metallic Nanolayers from Self-Assembled Lamellae of Diblock Copolymers. *Langmuir* **2005**, *21*, 3625–3628.
108. Bhaviripudi, S.; Reina, A.; Qi, J.; Kong, J.; Belcher, A. M. Block-copolymer Assisted Synthesis of Arrays of Metal Nanoparticles and Their Catalytic Activities for the Growth of SWNTs. *Nanotechnology* **2006**, *17*, 5080–5086.
109. Underhill, R. S.; Liu, G. J. Preparation and Performance of Pd Particles Encapsulated in Block Copolymer Nanospheres as a Hydrogenation Catalyst. *Chem. Mater.* **2000**, *12*, 3633–3641.
110. Abes, J. I.; Cohen, R. E.; Ross, C. A. Selective Growth of Cobalt Nanoclusters in Domains of Block Copolymer Films. *Chem. Mater.* **2003**, *15*, 1125–1131.
111. Chai, J. N.; Wang, D.; Fan, X. N.; Buriak, J. M. Assembly of Aligned Linear Metallic Patterns on Silicon. *Nat. Nanotechnol.* **2007**, *2*, 500–506.
112. Kern W. Overview and Evolution of Semiconductor Wafer Contamination and Cleaning Technology. In *Handbook of Semiconductor W.Wafer Cleaning Technology*; Kern, Ed.; Noyes Publications: Park Ridge, NJ, 1993; p 3.
113. Jaramillo, T. F.; Baeck, S.-H.; Cuenya, B. R.; McFarland, E. W. Catalytic Activity of Supported Au Nanoparticles Deposited from Block Copolymer Micelles. *J. Am. Chem. Soc.* **2003**, *125*, 7148–7149.
114. Lidin, R. A.; Andreyeva, L. L.; Molochko, V. A. *Reactivity of Inorganic Substance: Handbook*; Begell House Publication: Redding, CT, 1996.
115. Zhang, M.; Wang, Z.; Mo, M.; Chen, X.; Zhang, R.; Yu, W.; Qian, Y. A Simple Approach to Synthesize $KNiF_3$ Hollow Spheres by Solvothermal Method. *Mater. Chem. Phys.* **2005**, *89*, 373–378.
116. Gill, N. S.; Taylor, F. B. Tetrahalo Complexes of Dipositive Metals in the First Transition Series. *Inorg. Synth.* **1967**, *9*, 136–142.
117. Black, C. T.; Bezencenet, O. Nanometer-Scale Pattern Registration and Alignment by Directed Diblock Copolymer Self-Assembly. *IEEE Trans. Nanotechnol.* **2004**, *3*, 412–415.
118. Hammond, M. R.; Kramer, E. J. Edge Effects on Thermal Disorder in Laterally Confined Diblock Copolymer Cylinder Monolayers. *Macromolecules* **2006**, *39*, 1538–1544.
119. Sundrani, D.; Darling, S. B.; Sibener, S. J. Hierarchical Assembly and Compliance of Aligned Nanoscale Polymer Cylinders in Confinement. *Langmuir* **2004**, *20*, 5091–5099.
120. Ruiz, R.; Sandstrom, R. L.; Black, C. T. Induced Orientational Order in Symmetric Diblock Copolymer Thin Films. *Adv. Mater.* **2007**, *19*, 587–591.
121. Cheng, J. Y.; Zhang, F.; Smith, H. I.; Vancso, G. J.; Ross, C. A. Pattern Registration between Spherical Block-Copolymer Domains and Topographical Templates. *Adv. Mater.* **2006**, *18*, 597–601.
122. Huck, W. T. S. Effects of Nanoconfinement on the Morphology and Reactivity of Organic Materials. *Chem. Commun.* **2005**, *33*, 4143–4148.
123. Xiao, S. G.; Yang, X. M.; Edwards, E. W.; La, Y. H.; Nealey, P. F. Graphoepitaxy of Cylinder-Forming Block Copolymers for Use as Templates to Pattern Magnetic Metal Dot Arrays. *Nanotechnology* **2005**, *16*, S324–S329.
124. Cheng, J. Y.; Ross, C. A.; Smith, R. H.; Thomas, E. L. Templated Self-Assembly of Block Copolymers: Top-Down Helps Bottom-Up. *Adv. Mater.* **2006**, *18*, 2505–2521.
125. Hahn, J.; Webber, S. E. Graphoepitaxial Deposition of Cationic Polymer Micelles on Patterned SiO2 Surfaces. *Langmuir* **2004**, *20*, 1489–1494.
126. Naito, K.; Hieda, H.; Sakurai, M.; Kamata, Y.; Asakawa, K. 2.5-in. Disk Patterned Media Prepared by an Artificially Assisted Self-Assembling Method. *IEEE Trans. Magn.* **2002**, *38*, 1949–1951.
127. Lin, Y.; Boker, A.; He, J.; Sill, K.; Xiang, H.; Abetz, C.; Li, X.; Wang, J.; Emrick, T.; Su, L.; *et al.* Self-Directed Self-assembly of Nanoparticle/Copolymer Mixtures. *Nature* **2005**, *434*, 55–59.

128. Hammond, M. R.; Cochran, E.; Fredrickson, G. H.; Kramer, E. J. Temperature Dependence of Order, Disorder, and Defects in Laterally Confined Diblock Copolymer Cylinder Monolayers. *Macromolecules* **2005**, *38*, 6575–6585.
129. Loxley, A.; Vincent, B. Equilibrium and Kinetic Aspects of the pH-Dependent Swelling of Poly(2-vinylpyridine-co-styrene). *Microgels* **1997**, *275*, 1108–1114.
130. Fernández-Nieves, A.; Fernández-Barbero, A.; Vincent, B.; de la Nieves, F. J. Charge Controlled Swelling of Microgel Particles. *Macromolecules* **2000**, *33*, 2114–2118.
131. Xu, C.; Fu, X.; Fryd, M.; Xu, S.; Wayland, B. B.; Winey, K. I.; Composto, R. J. Reversible Stimuli-Responsive Nanostructures Assembled from Amphiphilic Block Copolymers. *Nano Lett.* **2006**, *6*, 282–287.
132. Xu, C.; Wayland, B. B.; Fryd, M.; Winey, K. I.; Composto, R. J. pH-Responsive Nanostructures Assembled from Amphiphilic Block Copolymers. *Macromolecules* **2006**, *39*, 6063–6070.
133. Boontongkong, Y.; Cohen, R. E. Cavitated Block Copolymer Micellar Thin Films: Lateral Arrays of Open Nanoreactors. *Macromolecules* **2002**, *35*, 3647–3652.